Journal of Power and Energy Engineering, 2026, 14(9), 1-17
https://www.scirp.org/journal/jpee
ISSN Online: 2327-5901
ISSN Print: 2327-588X

Control of Bidirectional DC-DC Converter for Electric Vehicle Charging Applications

Muhammad Zulhilmi Razali[1], Azrita Alias[1*], Jurifa Mat Lazi[1], Nurul Ain Mohd Said[1], Fazlli Patkar[1], Md Hairul Nizam Talib[1], Muhammad Zaid Aihsan[2]

[1]Faculty of Electrical Technology and Engineering, Universiti Teknikal Malaysia Melaka, Melaka, Malaysia
[2]Faculty of Electrical Engineering Technology, Universiti Malaysia Perlis (UniMAP), Perlis, Malaysia
Email: *azrita@utem.edu.my

How to cite this paper: Razali, M.Z., Alias, A., Lazi, J.M., Said, N.A.M., Patkar, F., Talib, M.H.N. and Aihsan, M.Z. (2026) Control of Bidirectional DC-DC Converter for Electric Vehicle Charging Applications. *Journal of Power and Energy Engineering*, **14**, 1-17.
https://doi.org/10.4236/jpee.2026.149001

Received: July 28, 2026
Accepted: September 8, 2026
Published: September 11, 2026

Abstract

The increasing adoption of electric vehicles (EVs) has created a growing demand for efficient bidirectional power conversion systems capable of supporting battery charging and energy transfer from the battery to the DC bus. This paper presents the design, mathematical modeling, and simulation of a non-isolated bidirectional buck-boost DC-DC converter for EV battery applications. The converter is designed for a rated power of 5 kW using a 350 V lithium-ion battery and a 450 V DC bus, with a switching frequency of 5 kHz. The passive components are analytically designed based on the specified operating conditions and continuous conduction mode (CCM) requirements. A closed-loop proportional-integral (PI) current controller is employed to regulate the battery current and enable bidirectional power flow between the battery and the DC bus. The converter performance is evaluated under different current-reference levels and during a dynamic transition between discharging and charging modes. The simulation results demonstrate effective current tracking and successful reversal of power flow, as indicated by the battery-current direction and corresponding state-of-charge response. The battery voltage remains stable during the operating-mode transition, while the inductor-current response is evaluated to verify CCM operation. The results demonstrate the feasibility of the proposed PI-controlled bidirectional DC-DC converter as a DC-side battery interface for EV charging and energy-transfer applications.

Keywords

Non-Isolated Bidirectional DC-DC Converter, Electric Vehicle, Battery Charging, Bidirectional Power Flow, PI Current Control, Lithium-Ion Battery, Continuous Conduction Mode

1. Introduction

The rapid growth of electric vehicles (EVs) has increased demand for efficient, compact, and controllable power electronic conversion systems that manage energy transfer between high-voltage battery packs and DC power buses. In EV powertrains and charging systems, DC-DC converters provide an important interface for voltage adaptation and controlled battery power flow. When bidirectional operation is incorporated, the converter can support energy transfer in both directions, enabling battery charging as well as battery-to-DC-bus power delivery for applications such as regenerative energy recovery and bidirectional energy management [1]-[3]. Recent studies have therefore placed considerable emphasis on bidirectional DC-DC converter topologies and their control strategies for EV and energy-storage applications.

Bidirectional DC-DC converters can generally be categorized into isolated and non-isolated configurations. Isolated converters provide galvanic isolation and are particularly attractive in applications where electrical safety and large voltage-conversion ratios are required. However, the additional transformer and switching components increase circuit complexity and influence converter size, cost, and control requirements. Non-isolated bidirectional converters offer a comparatively simple structure with fewer components and are therefore attractive for battery-to-DC-bus interfaces where galvanic isolation is not required at the investigated conversion stage [1] [4] [5]. Among these configurations, buck-, boost-, and buck-boost-derived bidirectional converters remain important candidates because of their ability to achieve controlled step-down and step-up operation while allowing reversal of power flow. Bidirectional buck-boost converters, in particular, have been investigated for battery-charging applications because they enable both step-down and step-up voltage conversion while supporting bidirectional power flow [4]. Among these configurations, buck-, boost-, and buck-boost-derived bidirectional converters remain important candidates because of their ability to achieve controlled step-down and step-up operation while allowing reversal of power flow.

In a bidirectional battery interface, the converter typically operates in different modes according to the required direction of energy transfer. During battery charging, energy is transferred from the DC bus toward the battery, whereas during battery discharging, the stored battery energy is transferred toward the DC bus. The switching converter must therefore provide not only the required voltage conversion but also controlled current flow during both operating modes. Current regulation is particularly important for lithium-ion batteries because the charging and discharging currents directly influence battery power transfer and state-of-charge (SOC) evolution. In EV battery chargers, controlled-current operation forms an important part of the battery-side power-conversion process.

Various control strategies have been investigated for DC-DC converters in EV and energy-storage applications, ranging from conventional proportional-integral (PI) controllers to more advanced, optimized techniques. For instance, optimization-based approaches have been employed to improve PI-controller performance in EV-related converter applications [6]. Although advanced and optimized approaches can provide improved dynamic performance and robustness, they may require greater computational complexity and additional tuning procedures. In contrast, PI control remains attractive as a baseline control strategy because of its simple structure, ease of implementation, and relatively low computational requirements. Current-controlled bidirectional converters have also been investigated specifically for lithium-ion battery applications, demonstrating the importance of accurate battery-current regulation during bidirectional operation [2].

For EV applications, current control can be implemented as an inner control function that regulates the inductor or battery current according to a specified reference. Previous work has demonstrated that current-controlled bidirectional DC-DC conversion can facilitate controlled energy transfer between an EV battery and a high-voltage DC bus, while more elaborate architectures may incorporate an additional outer voltage-regulation loop [5]. For the present investigation, a PI-based closed-loop current-control strategy is adopted to provide a straightforward assessment of current tracking and bidirectional power-flow reversal without introducing the additional complexity of advanced control algorithms.

This study, therefore, presents the design, mathematical modeling, and simulation of a 5 kW non-isolated bidirectional buck-boost DC-DC converter for an EV battery-to-DC-bus interface. The converter interfaces a 350 V nominal lithium-ion battery with a 450 V DC bus and operates at a switching frequency of 5 kHz. The passive components are analytically designed according to the selected operating conditions and continuous conduction mode (CCM) requirements. A closed-loop PI current controller is implemented to regulate the battery current during both directions of power transfer. The converter is evaluated at different current-reference levels and under a dynamic reversal between discharging and charging operations. Battery current tracking, battery-voltage response, SOC variation, DC-bus behavior, and inductor-current characteristics are examined to assess the effectiveness of the proposed system and to verify CCM operation.

2. Methodology

2.1. Converter Design and Mathematical Modeling

The bidirectional DC-DC converter considered in this study is designed as a non-isolated battery-to-DC-bus power interface for electric vehicle charging applications. The converter employs a synchronous half-bridge configuration that enables bidirectional energy transfer between a lithium-ion battery and a higher-voltage DC bus. During the charging operation, the converter operates in buck mode to transfer energy from the DC bus to the battery, whereas during the discharging operation, it operates in boost mode to transfer energy from the battery to the DC bus.

The converter is designed for a rated power of 5 kW with a nominal battery voltage of 350 V and a DC-bus voltage of 450 V. A switching frequency of 5 kHz is selected for the semiconductor switches. The main design specifications are summarized in **Table 1**.

Table 1. Design specifications of the bidirectional DC-DC converter.

Parameter	Symbol	Value
Rated power	P_r	5 kW
Nominal battery voltage	V_{bat}	350 V
DC-bus voltage	V_{dc}	450 V
Switching frequency	f_s	5 kHz
Switching period	T_s	200 µs
Rated battery current	$I_{bat,r}$	14.29 A
Allowable inductor-current ripple	ΔI_L	20% of rated current

The rated battery current is determined from the rated converter power and nominal battery voltage as

$$I_{bat,r} = \frac{P_r}{V_{bat}} = \frac{5000}{350} = 14.29\text{ A} \tag{1}$$

During battery charging, the converter operates in buck mode. Under ideal steady-state conditions, the nominal buck duty ratio is expressed as

$$D_{buck} = \frac{V_{bat}}{V_{dc}} = \frac{350}{450} = 0.778 \tag{2}$$

Therefore, the nominal duty ratio for buck operation is approximately 0.778.

During battery discharging, the converter operates in boost mode. The corresponding nominal duty ratio is

$$D_{boost} = 1 - \frac{V_{bat}}{V_{dc}} = 1 - \frac{350}{450} = 0.228 \tag{3}$$

The nominal duty ratio for boost operation is approximately 0.222.

The converter is designed to operate in continuous conduction mode (CCM), where the inductor current remains continuous throughout each switching period. An allowable peak-to-peak inductor-current ripple of 20% of the rated battery current is selected:

$$\Delta I_L = 0.2 I_{bat,r} = 0.2(14.29) = 2.86\text{ A} \tag{4}$$

For buck operation, the required inductance can be determined from

$$L_{min} = \frac{(V_{dc} - V_{bat}) D_{buck}}{\Delta I_L f_s} = \frac{(450 - 350) \times 0.778}{(2.86)(5000)} = 5.44 \times 10^{-3} \tag{5}$$

Hence, the calculated inductance is approximately 5.5 mH. The selected inductance limits the current ripple while supporting CCM operation at the rated operating point. The validity of the CCM assumption is subsequently verified from the simulated inductor-current waveform in the Results and Discussion section.

The DC-link capacitor is used to reduce the voltage ripple at the DC bus and to provide short-term energy buffering during converter switching. The capacitance is designed based on the allowable DC-bus voltage ripple during boost operation, which represents the battery-to-DC-bus power-transfer condition. The average DC-bus current at the rated power is calculated as

$$I_{dc} = \frac{P_r}{V_{dc}} = \frac{5000}{450} = 11.11\ \text{A} \tag{6}$$

The allowable DC-bus voltage ripple is selected as 1% of the nominal DC-bus voltage:

$$\Delta V_{dc} = (0.01)V_{dc} = 0.01(450) = 4.5\ \text{V} \tag{7}$$

For boost-mode operation, the minimum DC-link capacitance can be approximated by

$$C_{dc,min} = \frac{I_{dc} D_{boost}}{f_s \Delta V_{dc}} = \frac{11.11(0.222)}{(5000)(4.5)} = 109.6 \times 10^{-6} \tag{8}$$

A capacitance higher than the calculated minimum is selected to provide additional margin for DC-bus voltage-ripple suppression. Therefore, the selected DC-link capacitance is 220 μF. The selected value is approximately twice the calculated minimum capacitance and provides additional filtering margin during switching and bidirectional power-flow transition.

A capacitor is also connected across the battery-side terminal to attenuate high-frequency switching components and reduce the voltage ripple applied to the battery. Unlike the DC-link capacitor, the battery-side capacitor is sized based on the inductor-current ripple and the allowable battery-terminal voltage ripple. For the present design, the allowable battery-side voltage ripple is selected as 0.5% of the nominal battery voltage:

$$\Delta V_{bat} = (0.005)V_{bat} = (0.005)350 = 1.75\ \text{V} \tag{9}$$

Assuming a triangular inductor-current ripple, the minimum battery-side capacitance can be estimated as

$$C_{bat,min} = \frac{\Delta I_L}{8 f_s \Delta V_{bat}} = \frac{2.86}{8(5000)(1.75)} = 40.86 \times 10^{-6} \tag{10}$$

The required capacitance becomes 40.86 μF. A higher practical value is selected to provide sufficient filtering margin; we choose 100 μF. The selected battery-side capacitor reduces the high-frequency voltage ripple at the battery terminals without directly determining the average battery charging or discharging current. A small series resistance of 1×10^{-4} Ω was included in the passive branches to represent non-ideal component characteristics and facilitate numerical simulation. The calculated and selected converter parameters are summarized in **Table 2**.

Table 2. Calculated and selected design parameters of the bidirectional DC-DC converter.

Parameter	Symbol	Calculated Value	Selected Value
Rated battery current	$I_{bat,r}$	14.29 A	14.3 A
Buck duty ratio	D_{buck}	0.778	-
Boost duty ratio	D_{boost}	0.222	-
Current ripple	ΔI_L	2.86 A	-
Inductor	L	5.44 mH	5.5 mH
DC-link capacitor	C_{dc}	109.6 μF minimum	220 μF
Battery-side capacitor	C_{bat}	40.9 μF minimum	100 μF
Series resistor	R_s	-	1×10^{-4} Ω
Switching frequency	f_s	-	5 kHz

Figure 1 shows the MATLAB/Simulink implementation of the proposed non-isolated bidirectional DC-DC converter based on the calculated design parameters. The model was implemented with a discrete simulation step of 1 μs.

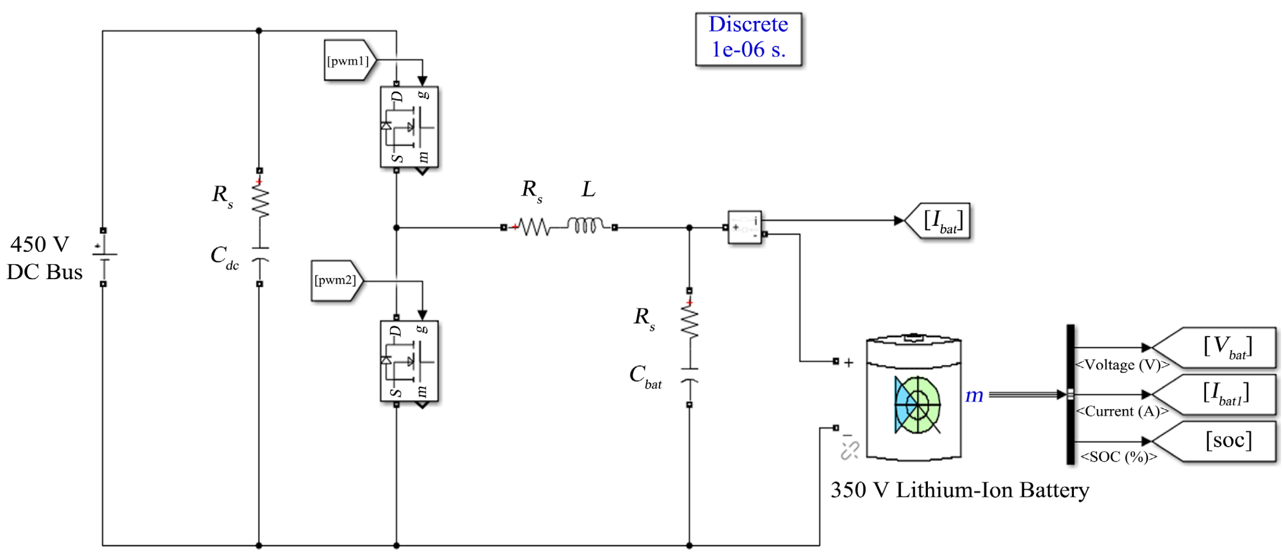

Figure 1. MATLAB/Simulink model of the bidirectional DC-DC power converter.

Battery Model and Parameters

A lithium-ion battery model was employed to represent the EV battery pack in the simulation. The battery was configured with a nominal voltage of 350 V and a rated capacity of 100 Ah, corresponding to a nominal energy capacity of 52.5 kWh. The battery energy capacity is expressed as

$$E_{bat} = V_{bat} Q_{bat} \quad (11)$$

where V_{bat} is the nominal battery voltage and Q_{bat} is the rated battery capacity.

Thus, $E_{bat} = (350)(100) = 35\ \text{kWh}$.

An initial SOC of 60% was selected to provide sufficient operating range for evaluating both charging and discharging conditions. The battery response time was set to 30 s, while temperature and aging effects were excluded to focus on the electrical behavior of the proposed converter. The battery parameters used in the simulation are summarized in Table 3.

Table 3. Battery model parameters.

Symbol	Components
Battery type	Lithium-Ion
Nominal voltage	350 V
Rated capacity	100 Ah
Initial SOC	60%
Fully charged voltage	407.4 V
Cut-off voltage	262.5 V
Nominal discharge current	43.48 A
Internal resistance	0.035 Ω
Capacity at nominal voltage	90.43 Ah
Battery response time	30 s

The battery terminal voltage varies with the battery operating condition rather than remaining fixed at its nominal value. Consequently, the measured terminal voltage may differ from the nominal value of 350 V during charging and discharging due to the battery discharge characteristics, SOC, internal resistance, and the direction and magnitude of the battery current. The SOC was obtained directly from the built-in lithium-ion battery model in MATLAB/Simulink based on the battery current and specified battery capacity; no separate SOC estimation algorithm was implemented in this study.

2.2. Converter Operating Modes

The proposed bidirectional DC-DC converter operates in two modes according to the direction of power flow between the DC bus and the EV battery. Referring to the converter topology in Figure 1, charging is achieved through buck operation, whereas discharging is achieved through boost operation. The direction of operation is determined by the battery-current reference applied to the closed-loop current controller. In this study, the battery-current sign convention is defined as

$$I_{bat} > 0 \text{ for charging}, \quad I_{bat} < 0 \text{ for discharging} \tag{12}$$

The general operating principle of a non-isolated bidirectional DC-DC converter is illustrated in Figure 2. The schematic is intended to provide a simplified representation of the bidirectional power-flow mechanism rather than the exact configuration of the proposed simulation model shown in Figure 1. In general, charging is achieved through buck operation with power transferred from the DC bus to the battery, whereas discharging is achieved through boost operation with power transferred from the battery to the DC bus.

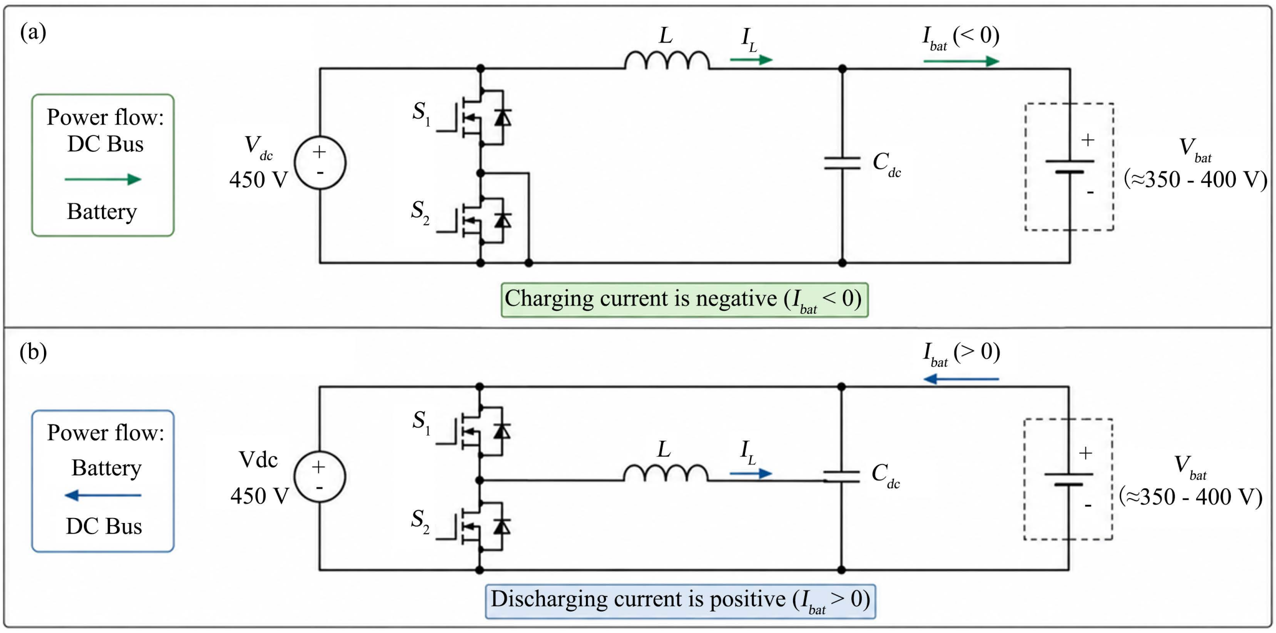

Figure 2. General operating principle of a bidirectional DC-DC converter: (a) charging (buck mode) and (b) discharging (boost mode).

2.2.1. Charging Operation (Buck Mode)

During charging, power is transferred from the 450 V DC bus to the EV battery. The converter operates in buck mode to reduce the DC-bus voltage to the required battery-side voltage while regulating the charging current according to the specified negative current reference. Energy transfer is controlled through the complementary switching action of the two semiconductor switches. During charging, power is transferred from the 450 V DC bus to the EV battery. Since the DC-bus voltage is higher than the battery voltage, the converter operates in buck mode. The two semiconductor switches are driven by complementary PWM signals to regulate the battery current according to the specified positive current reference. Based on the adopted sign convention, $I_{bat} > 0$ represents battery charging.

2.2.2. Discharging Operation (Boost Mode)

During discharging, the direction of power flow is reversed, with energy transferred from the EV battery to the higher-voltage DC bus. The converter therefore operates in boost mode, where the battery-side voltage is stepped up to the DC-bus voltage. Based on the adopted current sign convention, a negative battery current, $I_{bat} < 0$, represents a discharging operation. The battery current is regulated according to the specified positive current reference through the closed-loop current controller. The complementary switching action of the semiconductor switches controls the energy stored and released by the inductor, thereby enabling regulated power transfer from the battery to the DC bus.

2.3. Closed-Loop Cascaded Control Implementation

A closed-loop PI current controller is employed to regulate the battery current during both charging and discharging operations. The control structure uses the battery-current reference, I_{ref}, as the command input, while the measured battery current, I_{bat}, is fed back to the controller. The current error is defined as

$$e(t) = I_{ref}(t) - I_{bat}(t) \tag{13}$$

The current error is processed by a continuous-time PI controller to generate the duty-cycle command. The controller transfer function is expressed as

$$D(s) = \left(K_p + \frac{K_i}{s}\right) E(s) \tag{14}$$

where K_p and K_i are the proportional and integral gains, respectively, $E(s)$ represents the current error in the Laplace domain, and D represents the duty-cycle command supplied to the PWM generator. The PI controller output, representing the duty-cycle command, was constrained within the range $0 \le D \le 1$ prior to PWM generation, corresponding to a duty-cycle range of 0% - 100%.

The PI controller gains were determined using an iterative trial-and-error tuning approach. The proportional gain, K_p, was initially adjusted to obtain a sufficiently fast current-tracking response, while the integral gain, K_i, was subsequently tuned to minimize the steady-state current error. The gains were iteratively refined by observing the transient response, steady-state error, and current oscillations under both charging and discharging conditions. The same PI current controller is employed for both charging and discharging operations, with the direction of power flow determined by the sign of the reference current as defined in (12). The PI controller parameters used in this study are summarized in **Table 4**.

Table 4. PI current-controller parameters.

Control Loop	K_P	K_I	Switching Frequency	Duty Cycle Limit
Battery current PI controller	1.5	25	5 kHz	0 - 1

The duty-cycle command generated by the PI controller is subsequently converted into the PWM signal, PWM1, which is applied to the upper semiconductor switch, S1. The complementary switching signal, PWM2, is generated from PWM1 and applied to the lower switch, S2. This complementary switching arrangement ensures coordinated operation of the two semiconductor switches and enables controlled energy transfer through the converter inductor. The switching action is continuously adjusted according to the duty-cycle command produced by the PI controller in response to the battery-current error. Consequently, the measured battery current is regulated toward the specified reference current during both charging and discharging operations. The conceptual closed-loop current-control structure is illustrated in Figure 3.

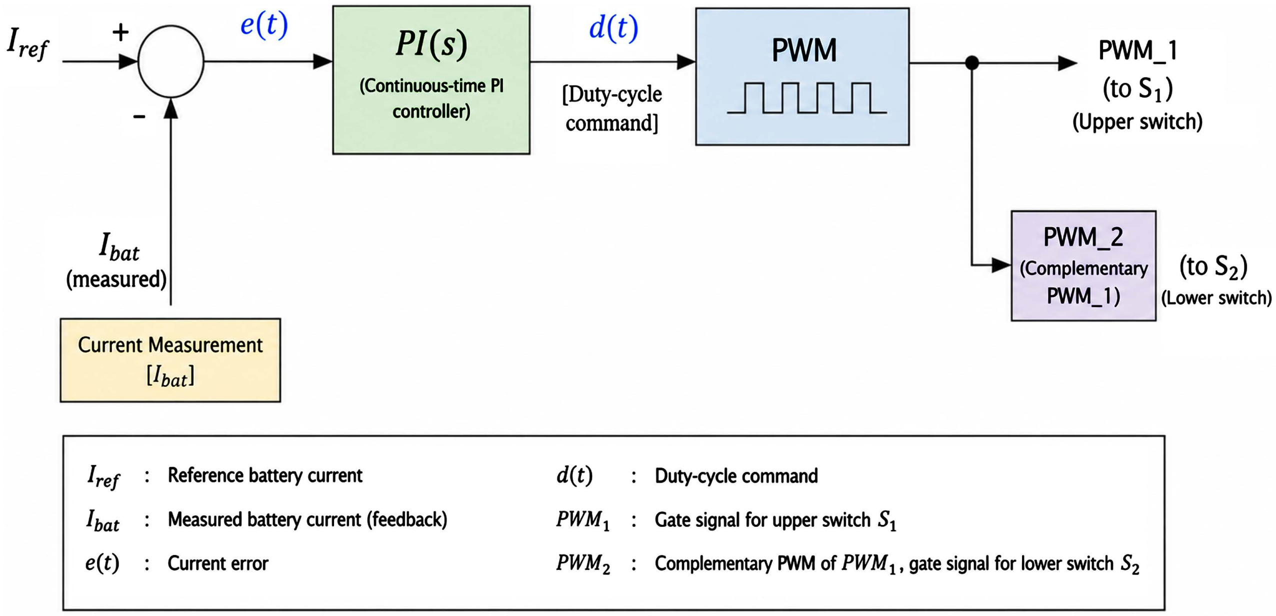

Figure 3. Closed-loop PI current-control structure of the bidirectional DC-DC converter.

The corresponding MATLAB/Simulink implementation of the current-control scheme is shown in Figure 4.

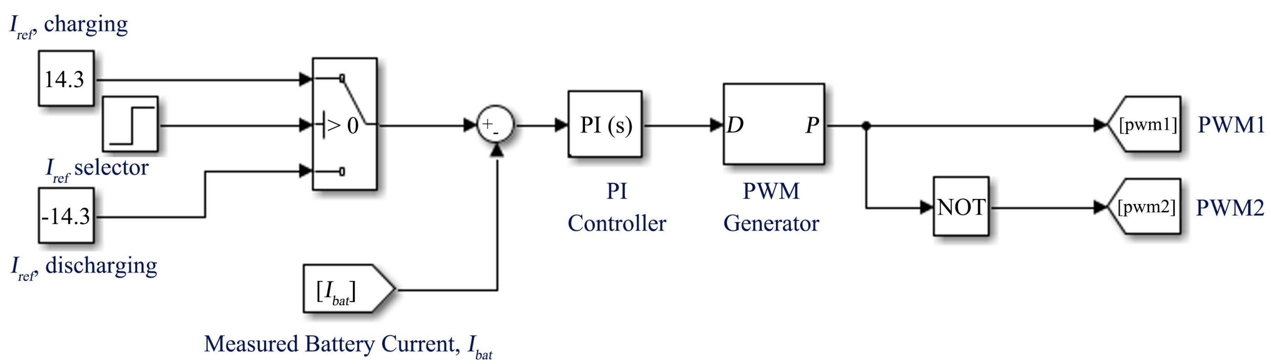

Figure 4. MATLAB/simulink implementation of the proposed PI current controller.

Figure 4 presents the MATLAB/Simulink implementation of the proposed closed-loop current-control scheme. The current-reference selector is used to switch between the predefined charging and discharging current references. The selected reference, I_{ref}, is compared with the measured battery current, I_{bat}, and the resulting current error is processed by the PI controller. The controller output determines the duty-cycle command for the 5 kHz PWM generator, which produces PWM1 for the upper switch. The complementary signal, PWM2, is generated from PWM1 and applied to the lower switch. This implementation enables a single PI current-control loop to regulate the battery current during both directions of power transfer.

During mode reversal, the current-reference selector changes the battery-current reference between the charging and discharging commands while the same PI current controller remains active. For the rated operating condition considered in this study, the current reference is constrained within −14.3 A to +14.3 A. No explicit integrator reset or hold mechanism is applied during the transition. The complementary switching signal, PWM2, is generated directly from PWM1.

An explicit dead-time circuit is not included in the present simulation model. Therefore, the present switching implementation is intended to evaluate the converter-level current-control behavior, while practical dead-time implementation and associated switching-device protection are beyond the scope of this simulation study.

3. Result and Discussion

The performance of the bidirectional DC-DC converter was evaluated under three battery-current reference levels of ±5 A, ±10 A, and ±14.3 A. The highest current magnitude of 14.3 A corresponds to the rated operating current of the 5-kW converter based on the nominal battery voltage of 350 V. The lower current levels were included to assess the current-control performance under different power-transfer conditions. For all simulation cases, the initial battery SOC was set to 60%, and the total simulation time was 10 s.

Based on the battery-current measurement orientation adopted in the simulation model, a negative battery current represents a discharging operation, whereas a positive battery current represents a charging operation. Accordingly, the converter was initially operated in discharging mode using negative current references. At $t = 5$ s, the reference polarity was reversed to the corresponding positive value to initiate the charging operation. This test condition was applied consistently at all three current levels to evaluate the bidirectional current-tracking capability and the battery response during mode reversal.

3.1. Bidirectional Current-Tracking and Battery Response

Figure 5 presents the converter response for a current-reference reversal from −5 A to +5 A. During the first 5 s, the measured battery current remains close to −5 A, demonstrating stable current regulation during discharging. At $t = 5$ s, the reference is changed to +5 A, and the battery current rapidly follows the new operating command and remains close to the desired charging current. No sustained oscillation is observed following the mode reversal.

The battery terminal voltage responds consistently to the change in current direction. During the discharging interval, the terminal voltage decreases gradually from approximately 377.6 V to 377.4 V. Following the transition to charging at $t = 5$ s, an increase in terminal voltage is observed, after which the voltage gradually rises during the charging interval. The SOC response provides further confirmation of the bidirectional power-flow behavior. The SOC decreases during discharging and reaches its minimum value at the mode-reversal instant before increasing during charging. The relatively small SOC variation is expected because of the 100 Ah battery capacity and the short simulation interval.

Figure 6 shows the corresponding responses for a current-reference reversal from −10 A to +10 A. The measured battery current closely follows the commanded value in both operating modes. Prior to $t = 5$ s, the current is maintained at approximately −10 A during discharging. Following the reference reversal, the current changes to approximately +10 A and remains regulated around the charging-current reference. The response indicates that the same PI controller can regulate the battery current at a higher current magnitude without requiring controller retuning.

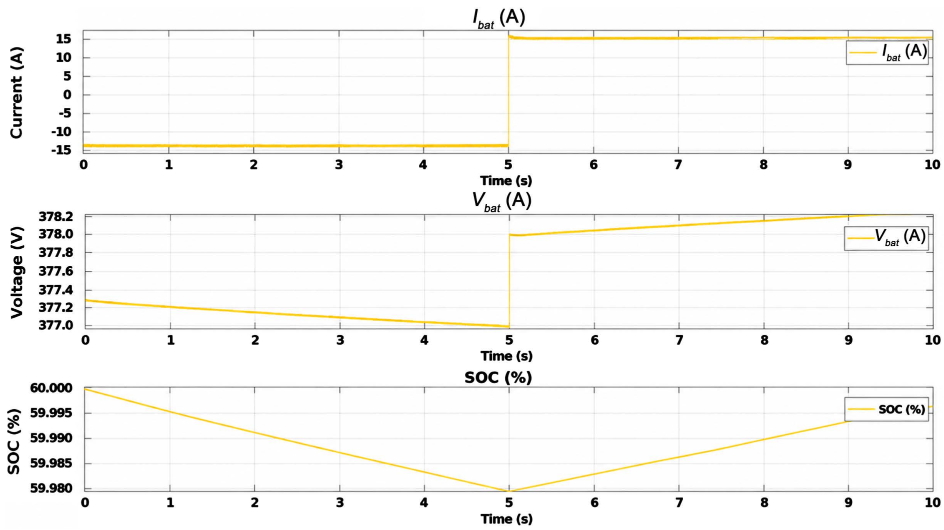

Figure 5. Battery responses during current-reference reversal from −5 A to +5 A: (a) battery current, (b) battery terminal voltage, and (c) SOC (%).

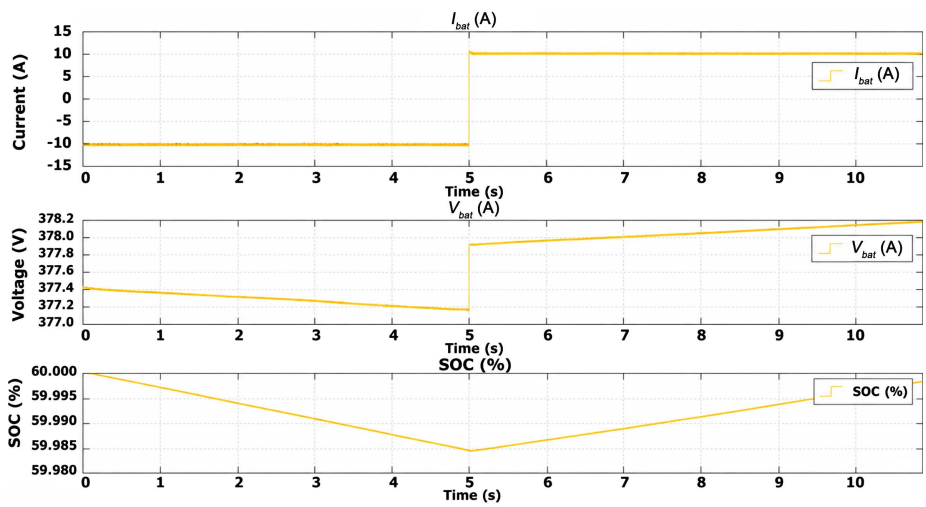

Figure 6. Battery responses during current-reference reversal from −10 A to +10 A: (a) battery current, (b) battery terminal voltage, and (c) SOC (%).

Compared with the ±5 A case, the higher current magnitude produces a more noticeable change in battery terminal voltage and SOC. The terminal voltage decreases during the discharging interval and exhibits an upward change when the converter switches to charging mode. Similarly, the SOC decreases more rapidly during discharging and subsequently increases during charging. These trends are consistent with the increased magnitude of battery current and, therefore, the higher rate of energy transfer.

Figure 7 presents the converter performance at the rated current-reference magnitude of 14.3 A. During the initial discharging interval, the battery current is regulated close to −14.3 A. At $t = 5$ s, the reference is reversed to +14.3 A, producing a rapid transition from discharging to charging operation. A small transient is observed immediately after the mode reversal before the current converges to the commanded charging level. The current subsequently remains stable around the reference value, demonstrating that the PI controller is capable of regulating the converter at its rated current condition.

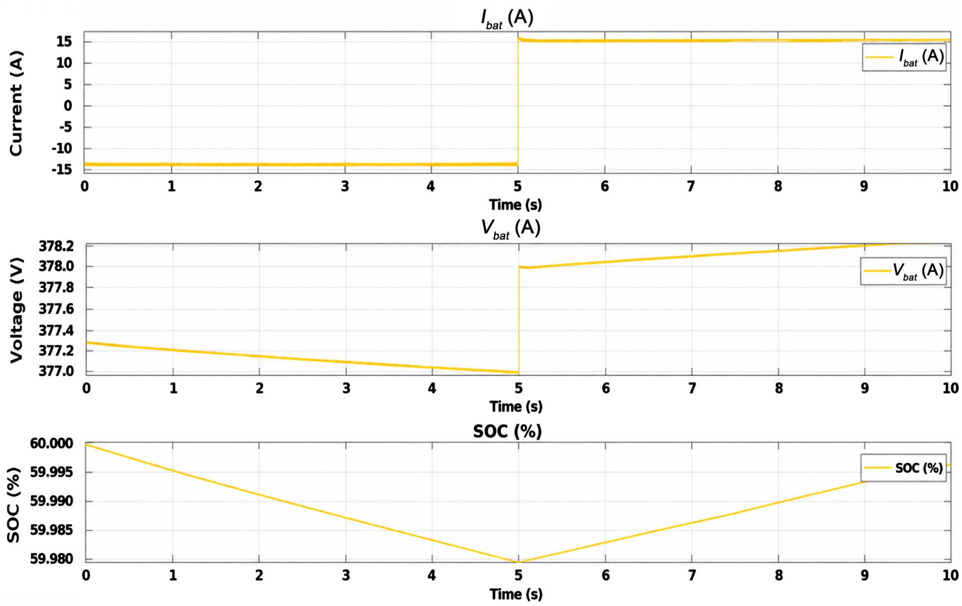

Figure 7. Battery responses during current-reference reversal from −14.3 A to +14.3 A: (a) battery current, (b) battery terminal voltage, and (c) SOC (%).

The effect of the higher current magnitude is also evident in the battery terminal voltage. During discharging, the voltage gradually decreases and reaches its lowest value immediately before the mode transition. When the current direction is reversed, the terminal voltage increases abruptly due to the change in current direction and subsequently rises gradually during charging. The SOC exhibits the same expected trend, decreasing from its initial value during discharging and increasing after the transition to charging. Among the three investigated operating conditions, the ±14.3 A case produces the largest SOC variation because it corresponds to the highest battery-current magnitude.

Overall, the results in Figures 5-7 demonstrate consistent bidirectional current regulation over the investigated range of ±5 A to ±14.3 A. The same PI controller successfully tracks the different current-reference levels and maintains stable operation before and after the discharging-to-charging transition. Increasing the current-reference magnitude results in greater changes in battery terminal voltage and SOC, as expected due to increased power transfer. More importantly, the measured battery current matches the commanded current direction and magnitude across all three operating conditions, demonstrating the effectiveness of the proposed closed-loop current-control strategy for the DC-bus battery interface investigated.

3.2. Switching and Inductor Current Characteristics

The switching behaviour and inductor-current characteristics were examined under the rated current condition of 14.3 A for both power-flow directions. Figure 8 and Figure 9 present the PWM signals applied to the upper and lower semiconductor switches together with the corresponding inductor current, I_L, during discharging and charging operations, respectively. The two gate signals exhibit complementary switching behaviour, whereby PWM2 is the logical complement of PWM1. This switching pattern is consistent with the PWM implementation described in Section 2.3.

Figure 8 shows the switching characteristics during rated discharging operation at $I_{ref} = -14.3\,\text{A}$. The inductor current remains negative and fluctuates around the rated discharging-current level. Although switching ripple is present, I_L remains continuous throughout the observed interval and does not approach or cross zero. This indicates that the converter operates in continuous conduction mode (CCM) under the rated discharging condition.

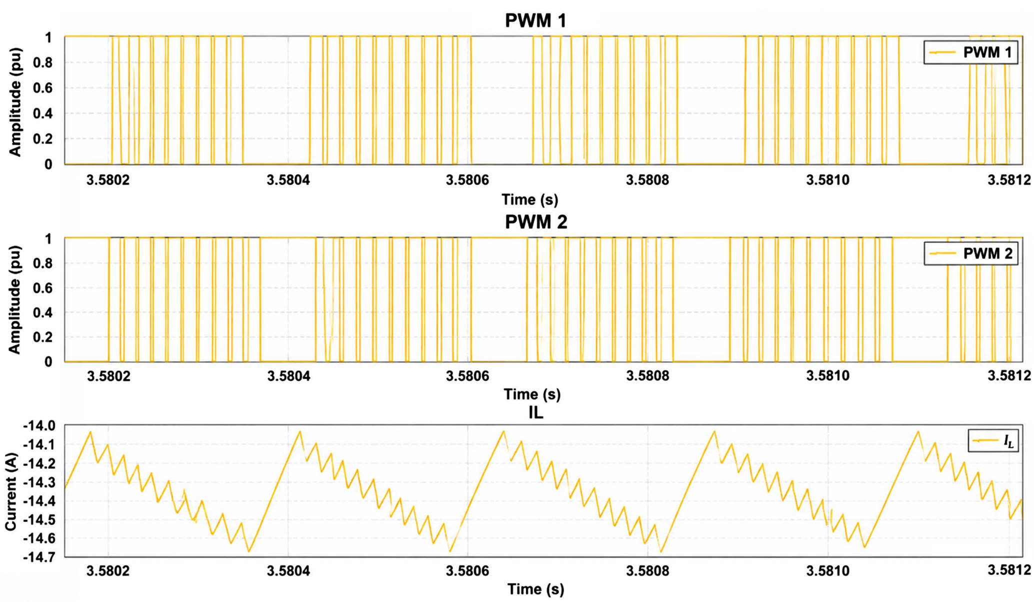

Figure 8. Switching and inductor-current characteristics during rated discharging operation at $I_{ref} = -14.3$ A: (a) PWM1, (b) PWM2, and (c) inductor current I_L.

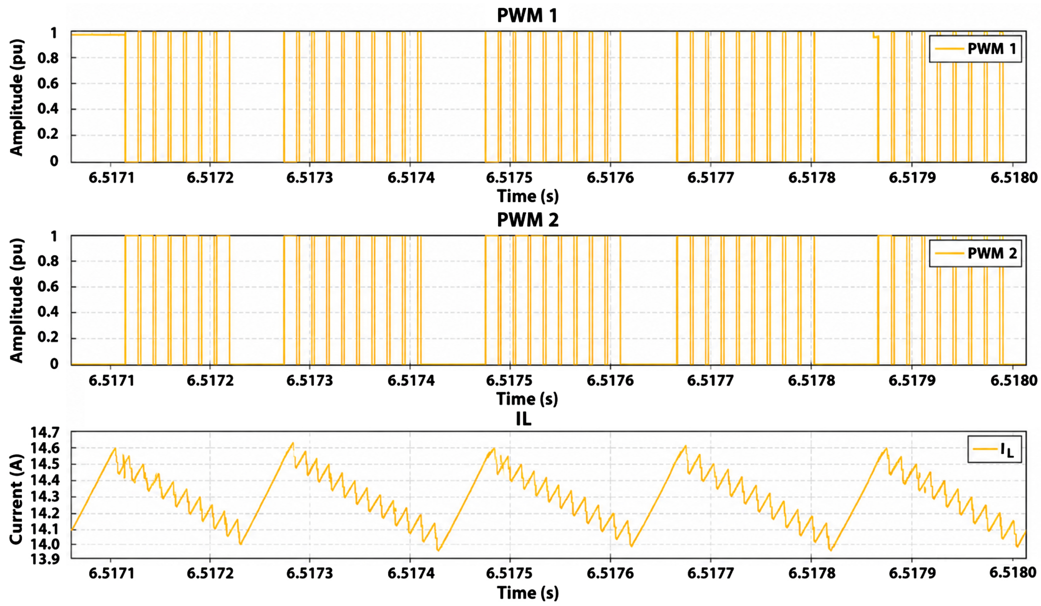

Figure 9. Switching and inductor-current characteristics during rated charging operation at I_{ref} = +14.3 A: (a) PWM1, (b) PWM2, and (c) inductor current I_L.

Figure 9 presents the corresponding behaviour during rated charging operation at $I_{ref} = +14.3\ \text{A}$. The polarity of the inductor current is reversed compared with the discharging condition, with I_L remaining positive around the rated charging-current level. Similar to the discharging case, the inductor current remains continuous throughout the switching interval without reaching zero. Therefore, CCM operation is also maintained during rated charging.

The results in **Figure 8** and **Figure 9** demonstrate that continuous inductor-current operation is maintained in both directions of power flow at the rated current condition. The current polarity changes according to the operating mode, while the complementary switching strategy remains unchanged. These results support the suitability of the selected converter parameters for bidirectional operation under the investigated rated condition.

4. Conclusions

This study presented the modeling and simulation of a non-isolated bidirectional buck-boost DC-DC converter for a DC-bus battery interface. A closed-loop PI current controller was implemented to regulate the bidirectional battery current, with complementary PWM signals used to drive the converter switches. The converter performance was evaluated at current-reference levels of ±5 A, ±10 A, and ±14.3 A, with the current direction reversed from discharging to charging at 5 s.

The simulation results demonstrate that the battery current follows the commanded reference under all investigated current levels and maintains stable operation following the mode reversal. The corresponding battery voltage and SOC responses are consistent with the direction and magnitude of battery current, with SOC decreasing during discharging and increasing during charging. At the rated current of ±14.3 A, the inductor current remains continuous in both power-flow directions, demonstrating CCM operation under the investigated rated condition. Overall, the results demonstrate the capability of the proposed converter and PI current-control scheme to provide controlled bidirectional power transfer between the DC bus and battery over the investigated operating range.

The present study is limited to the DC-side battery interface and does not include a grid-side converter, AC-grid model, or grid-side control. In addition, practical switching effects such as semiconductor nonidealities and dead time were not explicitly considered. Future work will therefore focus on experimental validation of the proposed converter and controller, including practical switching effects and evaluation under a wider range of battery and load operating conditions.

Author Contributions

Muhammad Zulhilmi: Conceptualization, Methodology, Simulation, Investigation, and Writing—Original draft. **Azrita Alias:** Conceptualization, Supervision, Methodology, Writing—review and editing, and Project administration. **Jurifa Mat Lazi:** Methodology, Validation, and Writing—review and editing. **Nurul Ain Mohd Said:** Validation, Formal analysis, and Writing—review and editing. **Fazlli Patkar:** Investigation, Resources, and Writing—review and editing. **Md Hairul Nizam Talib:** Methodology, Validation, and Writing—review and editing. **Muhammad Zaid Aihsan:** Formal analysis, Visualization, and Writing—review and editing. All authors have read and approved the final version of the manuscript.

Acknowledgements

The authors would like to express their sincere gratitude to Universiti Teknikal Malaysia Melaka (UTeM), the Faculty of Electrical Technology and Engineering, for their support and contributions.

Conflicts of Interest

The authors declare no conflicts of interest regarding the publication of this paper.

References

[1] Tong, Y., Salhi, I., Wang, Q., Lu, G. and Wu, S. (2025) Bidirectional DC-DC Converter Topologies for Hybrid Energy Storage Systems in Electric Vehicles: A Comprehensive Review. *Energies*, **18**, Article 2312. https://doi.org/10.3390/en18092312

[2] Kumar, M.P., Durgam, R. and Krishan, R. (2025) Robust Current Control in Lithium-Ion Battery with a Bidirectional Buck-Boost Converter. 2025 *IEEE* 1*st International Conference on Smart and Sustainable Developments in Electrical Engineering* (*SSDEE*), Dhanbad, 28 February-2 March 2025, 1-6. https://doi.org/10.1109/ssdee64538.2025.10969044

[3] Ragasudha, C.P. and Hemamalini, S. (2024) Performance Analysis of a High Gain Bidirectional DC-DC Converter Fed Drive for an Electric Vehicle with Battery Charging Capability during Braking. *IEEE Access*, **12**, 14499-14511. https://doi.org/10.1109/access.2024.3357726

[4] Benlahbib, B., Dahbi, A., Fares, B., Lakhdari, A., Bouarroudj, N., Mekhilef, S., *et al.*

(2023) An Experimental Investigation Design of a Bidirectional DC-DC Buck-Boost Converter for PV Battery Charger System. *International Journal of Power Electronics and Drive Systems* (*IJPEDS*), **14**, 2362-2371. https://doi.org/10.11591/ijpeds.v14.i4.pp2362-2371

[5] González-Castaño, C., Restrepo, C., Kouro, S., Vidal-Idiarte, E. and Calvente, J. (2021) A Bidirectional Versatile Buck-Boost Converter Driver for Electric Vehicle Applications. *Sensors*, **21**, Article 5712. https://doi.org/10.3390/s21175712

[6] Kancherla, A.B., Prasad, N.B. and Kishore, D.R. (2023) PV-Based Grid Integrated EV with GWO Optimized PI Controller for Boost Integrated Luo Converter. *Journal of the Institution of Engineers* (*India*): *Series B*, **105**, 309-321. https://doi.org/10.1007/s40031-023-00968-y